Supporting Information

Real-Time Elucidation of Catalytic Pathways in CO Hydrogenation on Ru

J. LaRue[†‡§ ∥ *] O. Krejčí,[‡⊥#] L. Yu,[▽] M. Beye,[°] M. L. Ng,[†] H. Öberg,[‡] H. Xin,[▽] G. Mercurio,[◆] S. Moeller,[¶] J. J. Turner,[¶] D. Nordlund,[◎] R. Coffee,[¶] M. P. Minitti,[¶] W. Wurth,[◆ʃ] L. G. M. Pettersson,[‡] H. Öström,[‡] A. Nilsson,[‡] F. Abild-Pedersen,[†] H. Ogasawara[◎*]

†SUNCAT Center for Interface Science and Catalysis, SLAC National Accelerator Laboratory, 2575 Sand Hill Road, Menlo Park, California 94025, USA

‡Department of Physics, AlbaNova University Center, Stockholm University, SE-10691 Stockholm, Sweden

§Schmid College of Science and Technology, Chapman University, One University Drive, Orange, California 92866, USA

∥ Fritz-Haber Institute of the Max-Planck-Society, Faradayweg 4-6, D-14195 Berlin, Germany

⊥Charles University in Prague, Faculty of Mathematics and Physics, Department of Surface and Plasma Science, V Holešovičkách 2, 180 00, Prague, Czech Republic

#Institute of Physics of the Czech Academy of Sciences, Cukrovarnická 10, 162 53, Prague, Czech Republic

∇SUNCAT Center for Interface Science and Catalysis, Department of Chemical Engineering, Stanford University, Stanford, California 95305, USA

○Helmholtz Zentrum Berlin für Materialien und Energie GmbH, Albert-Einstein-Strasse 15, D-12489 Berlin, Germany

◆University of Hamburg and Center for Free Electron Laser Science, Luruper Chausse 149, D-22761 Hamburg, Germany

¶Linac Coherent Light Source, SLAC National Accelerator Laboratory, 2575 Sand Hill Road, Menlo Park, California 94025, USA

⊗Stanford Synchrotron Radiation Lightsource, SLAC National Accelerator Laboratory, 2575 Sand Hill Road, Menlo Park, California 94025, USA

∫DESY Photon Science, Notkestrasse 85, 22607 Hamburg, Germany

AUTHOR INFORMATION

Corresponding Authors

J. L. LaRue (larue@chapman.edu) and H. Ogasawara (hirohito@slac.stanford.edu).

Supporting Information Contents:

I. Experimental Methods: Laser Pump X-ray Probe Experiments

The clean Ru(0001) sample was prepared through cycles of 5 minutes of Ne ion sputtering (P_{Ne} = 7 x 10^{-6} Torr), 5 minutes of O_2 cleaning (P_{O2} = 2 x 10^{-7} Torr, T = 1200 K), and 2 flash anneals (T = 1500 K) under ultrahigh vacuum conditions. The (CO + H)/Ru(0001) surface was prepared by exposing the clean Ru(0001) surface to a background pressure of 5 x 10^{-9} Torr CO and 2 x 10^{-8} Torr H_2 at a temperature of 500 K. The surface was then allowed to cool down to the experimental running temperature of 100 K while the background pressures of both CO and H_2 remained constant at the pressures specified above. Under background dosing conditions, the CO molecules still adsorb on ontop sites, while the H_2 molecules dissociate into atomic H on the surface, which reside preferentially in the fcc three-fold hollow sites.(1-4) Optical pump, x-ray probe experiments were performed using the SSE endstation[8] at the soft x-ray (SXR) beam line of the Linac Coherent Light Source (LCLS) at the SLAC National Accelerator Laboratory.(6-8)

The pump-probe setup is described in the supplementary online materials of reference.(6) X-ray absorption spectra (XAS) and x-ray emission spectra (XES) were recorded in partial fluorescence yield mode. We monitored the intensity variation in the O K-edge x-ray emission as a function of the incident photon energy using a grating spectrometer.(5) The photon energy was continuously scanned through 527.0-541.0 eV, i.e. near the O K-edge, with synchronous beamline monochromator energy and FEL electron energy scans. Since there is an inborn linkage between XAS and XES, the O K-edge XAS spectra were measured in partial fluorescent yield mode by monitoring the integrated intensity variation of the O K-edge XES as a function of the incident energy. Since one data point in O K-edge XAS corresponds to the total integrated intensity of O K-edge XES measured at particular photon energy, there is inherently less noise in XAS than XES, which allows quantitative analysis.

The x-ray pulses generated by LCLS had a pulse length of less than 80 fs and were monochromatized using a 100 line/mm grating at an exit slit of 115 μm providing a resolving power of E/ΔE=3000 and a photon flux onto the sample of 1.3×10^{10} photons/pulse.(9,10) Reference O1s spectra of the (CO + H) / Ru(0001) surface were recorded at beamline 13-2 of the Stanford Synchrotron Radiation Lightsource (SSRL) at the SLAC National Accelerator Laboratory. Optical laser pulses at a wavelength of 400 nm and pulse length of about 70 fs were used to drive the reaction. The pulse energy of the 400 nm laser was set close to the damage threshold of the Ru(0001) surface and the absorbed fluence was estimated to be 130 J/m^2 (1/e^2). The optical laser and x-ray laser were collinear with respect to each other and at 2° grazing incidence with respect to the sample surface. To ensure that the x-ray beam was entirely overlapped by the 400 nm laser beam, the x-ray beam was focused to 20 μm at the position of the sample, whereas the 400 nm laser beam was set to a focus of 42 ± 2 μm FWHM. The x-ray laser was operated at 30 Hz, while the 400 nm laser was operated at 10 Hz to provide unpumped reference spectra between each pumped laser shot. The sample was scanned at a speed of 0.8 mm/s during experiments, separating the laser spots on the sample by 80 μm, so that the laser continuously excited fresh spots on the sample. The time elapsed between consecutive 400 nm shots on any given spot on the sample was ~40 seconds. This was enough time for H and CO to re-adsorb back onto the surface from the background pressures of H$_2$ and CO. The time-resolution of the pump-probe experiment is dependent on the inherent pulse width of the optical and free-electron laser pulses and the relative timing between these. Temporal overlap was determined using the optical reflectivity of a Si$_3$N$_4$ sample.(11) The relative timing between the pulses was monitored for each shot using a non-destructive optical x-ray cross-correlator(12) and

corrected for during data analysis. Based on the respective pulse lengths we estimate a time-resolution of 100 fs.

II. Experimental Methods: Laser-Induced Desorption Mass Spectrometry Experiments

The clean Ru(0001) sample was prepared through cycles of 5 minutes of Ar ion sputtering (P_{Ne} = 1 x 10^{-6} Torr), 5 minutes of O_2 cleaning (P_{O2} = 4 x 10^{-7} Torr correcting for ion gauge sensitivity, T = 1200 K), and 3 flash anneals (T = 1500 K) under ultrahigh vacuum conditions. The surface was LN_2 cooled down to a temperature of ~110 K. The (CO + H)/Ru(0001) surface was prepared by exposing the clean Ru(0001) surface to 60 L of H_2 (2 x 10^{-7} Torr, 150 seconds), followed by 20 L of CO (2 x 10^{-7} Torr, 100 seconds). The H_2 was dosed before CO, which would otherwise have inhibited H_2 dissociative adsorption. These conditions were found to give similar results as the optical pump, x-ray probe experiments.

The femtosecond laser-induced experimental setup has been detailed in reference.(13) Briefly, a commercial Ti:sapphire amplifier system providing 800 nm, 50 fs laser pulses at a repetition rate of up to 1 kHz and a pulse energy of up to 2.5 mJ/pulse was used. In the present experiment the repetition rate was set to 100 Hz and the laser was frequency-doubled to produce a fluence of 100 J/m^2 at 400 nm. The laser was used to initiate the reaction and a quadrupole mass spectrometer (QMS) was used to measure the masses of the gas phase product distribution. Masses 29 (CHO) and 30 (CH_2O) were of primary interest. Each fresh spot on the sample was irradiated with 50 laser shots and the product distribution for each shot was recorded.

CHO desorption is favoured over CH_2O desorption by an order of magnitude. After the first laser shot, the reaction yield for both CH_2O and CHO decreases by ~90%. Under similar laser fluences at 400 nm, it has been shown that ~1/3 of the adsorbed CO will desorb from a saturated CO/Ru(0001) surface on the first laser shot.(13) As this does not explain the 90% decrease in

CH$_x$O species, we postulate that the surface is largely depleted of H due to H + H recombinative desorption in the first laser shot. Previous 2-pulse correlation experiments for H + H associative desorption on Ru(0001) using 800 nm laser pulses indicate that the energy for the H + H reaction channel is dissipated within 1.1 ps (FWHM)[17]. This is within the < 3 ps timescale for the observed CH$_x$O signature in x-ray absorption spectra and would be consistent with H depletion on the surface. Further, for high laser fluences at 800 nm in reference,(14) the authors found that most of the H is desorbed in the first laser shot. We believe that we were in a similar fluence regime at 400 nm for the optical pump, x-ray probe experiments.

III. Computational Methods: Spectrum Calculations

For the O K-edge x-ray absorption spectroscopy (XAS) and the x-ray emission spectroscopy (XES) simulations, we used the real-space-grid GPAW code,(15,16) which is based on density functional theory (DFT) and the projector-augmented-wave approach.(17) The exchange-correlation interaction was calculated via the revised Perdew-Burke-Ernzerhof (RPBE) functional.(18) The XAS spectra were computed via the Haydock recursion method(19) using 2000 Lanczos vectors with a half-core hole(20) situated on one oxygen atom. To obtain the absolute energy scale for the XAS spectra, we carried through the Δ Kohn-Sham (ΔK-S) calculations according to the procedure suggested by Ljungberg et al..(21) The XAS cross sections were broadened by Gaussian functions with a FWHM of 0.5 eV and Lorentzian functions with a broadening parameter of δ=0.3 eV. The emission spectra were obtained from the ground state orbitals(22) and were broadened by Gaussian functions with a FWHM of 1.0 eV. The simulated experimental-like XAS and XES cross sections for the adsorbed molecules were obtained using $0.5x + 0.5y + 1.0z$, where x, y and z are cross sections in the x, y and z direction, respectively.

For spectrum calculations of the products, we used a four-layered Ru slab, while the CO →

CHO transition state spectra were obtained with a slab containing three Ru layers; the difference

between simulated spectra on three- and four- layer slabs is marginal. Both Ru slabs have cell

parameter $a = 2.75$ Å and $c = 4.37$ Å and contained 20 Å of vacuum above them. The two top

layers of Ru, together with adsorbates, were allowed to relax during geometry optimizations. For

all the simulations we employed a grid spacing of 0.2 Å. For the XAS simulation, a 6×6

supercell was used to avoid interaction between core-holes and the Brillouin zone was

represented by the Γ-point only. The emission spectrum calculations were performed on a

smaller 2×2 supercell with Monkhorst-Pack(23) 4×4×1 k-point sampling of the Brillouin zone. It

was found that presence of hydrogen atoms on the Ru surface has negligible effect on the

simulated spectra.

The theoretical XAS spectra plotted in Figure 1 and Figure S7 were slightly shifted, so the $2\pi^*$

peak of the CO(ads) adsorbed in the on-top position would fit to the experimental data obtained

with negative probe delay (CO + H on the Ru surface). The resulting blue-shift for the products

on slabs containing four Ru-layers was 0.08 eV, while for the three-layer slab with transition

state system it was 0.21 eV. These discrepancies between theory and experiment are within the

precision of the ΔK-S approach, which is up to 1 eV depending on the exchange-correlation

functional used and the system.(19) The XES absolute energy scale was obtained by means of

shifting the simulated 5σ and 1π peak of CO/Ru to a Gaussian function fit of the experimental

5σ and 1π main peak between 522 and 526 eV. The same shift was applied for both the four- and

three-layer Ru slabs.

To find the minimum reaction and transition state path for CO hydrogenation, nudged elastic

band (NEB) calculations(24,25) were performed. For these calculations, the slab consisting of 3

layers of Ru and 20 Å of vacuum above it was used in order to reduce computational cost. We employed Monkhorst-Pack(23) 4×4×1 k-point sampling per 2×2 supercell. The force criterion for the geometry optimizations in the NEB calculations was set to 0.01 eV/Å and the lowest Ru layer was fixed during the optimization. The initial geometry had the CO(ads) at the "ontop" position and one hydrogen atom at "hcp" position in the 2×2 Ru cell giving a coverage of ¼ monolayer for both H(ads) and CO(ads), while the final geometry consisted of CHO lying down with carbon atom in almost "on-top" position.

IV. Computational Methods: Free-Energy Calculations

All electronic structure calculations were performed using the plane-wave-based density functional theory program PWSCF (Quantum-ESPRESSO)(26) with the ultrasoft Vanderbilt pseudopotential method and the BEEF exchange-correlation functional.(27) A cutoff energy of 500 eV for the wave functions and 5000 eV for the charge density were used. An excess of at least 20 bands was used in each of our calculations. The Ru(0001) slab model was built in a rectangular supercell using four layers of atoms with the bottom two layers fixed during structural relaxations. The size of the supercell was set as 1×2 for simulating the formation of H_2(ads) and CHO(ads) and 2×2 for that of CH_2O(ads). The Monkhorst-Pack scheme was used for sampling the Brillouin zone.(23) A k-point grid of 6×6×1 was used for the 1×2 supercell, and 3×6×l for the 2×2 supercell. The vacuum thickness of all models was set as ~ 10 Å.

The transition states of the formation of H_2(ads), CHO(ads), and CH_2O(ads) on the Ru(0001) surface were searched using the Nudged Elastic Band (NEB) method.(24,25) For the desorption of H_2(ads), CHO(ads), and CH_2O(ads) to the gas phase, the reaction pathways were calculated using constrained optimization along the reaction coordinate.

The free energies of reaction intermediates and transition states on the surface were calculated by:

$$G = E_{tot} + ZPE + H_{vib} - TS_{vib} \qquad (S.1)$$

Where E_{tot} is the density functional theory calculated total energy, ZPE is the zero-point energy, and H_{vib} and S_{vib} are the enthalpy and entropy parts from non-imaginary vibrations of the species on the surface. It should be mentioned that for the intermediate states concerning the reaction of CO(ads) and H(ads) to form CHO(ads) and CH_2O(ads) under different temperatures, the contribution of vibrations in the free energy between these states is marginal due to their comparable vibrational frequencies, see Supplementary Table 1. For simplicity, we just used the 0 K values. This does not affect the calculation of free energy barriers, in which both the initial state and the transition state include the contribution of the vibrations in the free energy.

The free energy change for the desorption of CHO and CH_2O was calculated using the potential (G(s)) of mean force,(28,29) which can be described as:

$$G(s) = V_0(s) - k_B T \, \Sigma_{all\ q,\ q \neq s} \ln \int \exp[-V(q,s) / k_B T] \, dq \qquad (S.2)$$

G(s) is the free energy of the system along the reaction coordinate, s. The free energy of the system at 0 K and 2000 K is shown in Supplementary Figure S2. At 0 K, it is simply the minimum energy potential, $V_0(s)$. At non-zero T, the contribution of entropy to the free energy was calculated based on the interaction potential, V(q,s), along all of the remaining coordinates orthogonal to s, as described in equation (S.2). V(q,s) is the interaction potential for mode q relative to $V_0(s)$. In the desorption reaction path, we considered five degrees of freedom for the adsorbate in each image including three rotations (2 cartwheel modes and 1 helicopter mode) and two translations (in the x and y directions) and calculated the interaction potential along them.

The internal vibrational modes have negligible contributions to the free energy change and are not taken into account here. More details about the approach can be found in Reference 30.

Ab Initio molecular dynamics (AIMD) simulations were carried out in the NVT ensemble using Langevin dynamics implemented in the Atomic Simulation Environment (ASE). The interatomic forces as a result of the potential energy surface were obtained on-the-fly from QUANTUM ESPRESSO(26) with 500 eV kinetic energy cutoff and the BEEF exchange-correlation functional.(27) In all calculations the time steps were set at 2 fs. In the Langevin equation, an electronic friction term against the velocity of atoms and a stochastic force via coupling to a heat bath are added into the equation of motion. The crucial parameter in this formalism is the electronic friction that governs the energy transfer. For the purpose of thermalization, the friction term is set to 0.002 atomic units without further effort to obtain *ab initio* friction from electron-phonon calculations.

The formation of CHO(ads) was also simulated using the AIMD calculations, in which an initial velocity was given to a CO(ads) and its adjacent H(ads) to kick them moving toward each other. The directions of the initial velocities of the kicked CO(ads) and H(ads) were set based on the frustrated rotation mode of CO(ads) and translational mode of H(ads). The values of the initial velocities were given according to the Maxwell-Boltzmann distribution under finite temperature. Results show that CHO(ads) was easily formed at ~50 fs with an initial temperature of 2500 K for Ru and H(ads), and 500 K for CO(ads). The formation trajectory of CHO(ads) is shown in Supplementary Figure S5.

V. Arrhenius Expression and Fraction of Reacting Molecules

The Maxwell-Boltzmann distribution in energy is given by:

$$f_E(E)dE = N\sqrt{E}\exp\left(-\frac{E}{k_B T}\right)dE \qquad (S.3)$$

The normalization constant N is obtained from:

$$1 = \int_0^\infty f_E(E) dE = N \int_0^\infty \sqrt{E} \exp\left(-\frac{E}{k_B T}\right) dE \qquad (S.4)$$

Substitute $u^2 = \dfrac{E}{k_B T}$ and $dE = 2k_B T u \, du$:

$$1 = 2N(k_B T)^{3/2} \int_0^\infty u^2 \exp(-u^2) du = 2N(k_B T)^{3/2} \left\{ -\frac{1}{2}\left[u\exp(-u^2)\right]_0^\infty + \frac{1}{2}\int_0^\infty \exp(-u^2) du \right\} = N(k_B T)^{3/2} \sqrt{\pi}$$

(S.5)

The normalization is thus:

$$N = \frac{1}{\sqrt{\pi}(k_B T)^{3/2}} \qquad (S.6)$$

The minimum temperature, T_{min}, with the kinetic energy corresponding to a thermal energy of

at least the energy required to form surface adsorbed CHO (1.2 eV) is:

$$T_{min} = 1.2[eV] / k_B \approx 14000 \, [K] \qquad (S.7)$$

Next, we integrate the Maxwell-Boltzmann distribution from the corresponding minimum

energy $k_B T_{min}$ with the average kinetic energy at 500 K:

$$\frac{1}{\sqrt{\pi}(k_B T)^{3/2}} \int_{14000 k_B}^\infty \sqrt{E} \exp\left(-\frac{E}{500 k_B}\right) dE \qquad (S.8)$$

With the above substitution we get:

$$u_{min}^2 = \frac{14000 k_B}{500 k_B} = 28 \Rightarrow u_{min} \approx 5.29 \qquad (S.9)$$

And a multiplicative factor of $2(k_B T)^{3/2}$ so the fraction is given by the integral:

$$\frac{2}{\sqrt{\pi}} \int_{5.29}^\infty u^2 \exp(-u^2) du = \frac{2}{\sqrt{\pi}}\left\{ -\frac{1}{2}\left[u\exp(-u^2)\right]_{5.29}^\infty + \frac{1}{2}\int_{5.29}^\infty \exp(-u^2) du \right\} = \frac{1}{\sqrt{\pi}}\left\{ 5.29\exp(-28) + erfc(5.29) \right\}$$

(S.10)

This evaluates to $\approx 3.6 \cdot 10^{-12}$ as the fraction at thermal equilibrium at 500 K having enough energy to surmount the barrier of 1.2 eV. The rate, R, of conversion is given by the Arrhenius expression:

$$R = \nu_0 \exp\left(-\frac{E_a}{k_B T}\right) \qquad (S.11)$$

Which at 500 K results in 8 conversions per site per second, assuming a standard attempt rate of 10^{13}, while at 2000 K the rate becomes $9.5 \cdot 10^9$ conversions per site per second. The fraction of molecules that at any given time at the higher temperature 2000 K can cross the barrier (u_{min}=2.646) is found from:

$$\frac{2}{\sqrt{\pi}} \int_{2.646}^{\infty} u^2 \exp\left(-u^2\right) du = \frac{2}{\sqrt{\pi}}\left\{-\frac{1}{2}\left[u\exp\left(-u^2\right)\right]_{2.646}^{\infty} + \frac{1}{2}\int_{2.646}^{\infty}\exp\left(-u^2\right)du\right\} = \frac{1}{\sqrt{\pi}}\left\{2.646\exp\left(-7\right)+erfc\left(2.646\right)\right\}$$
$$(S.12)$$

This evaluates to ~0.24%.

VI. XES Difference Spectra

The difference between the unpumped and pumped XES spectra is shown in Figure S6 where the total integrated intensity of XES spectra was normalized to the incoming x-ray photon flux. Therefore, the integrated spectral intensity of XES in Figure 1c corresponds to the XAS intensity integrated over the x-ray energy range 530.2 to 533.0 eV. Since there is an increase in XAS intensity after the laser pump, the integrated intensity of XES after the pump is larger than that before the pump. The removal of CO due to the CH_xO formation can lead to a negative intensity in the difference spectrum. However, there is a peak position change in the XES peak of CO, especially for the 4σ and 5σ states, due to the translational excitation at high temperature after the laser excitation. See Figure S7, CO(ads) NEB and Reference 31. This results in positive and negative contributions from the XES of CO itself which smears out changes in the difference

spectrum in this region. This limits the quantitative interpretation of XES in the x-ray emission energy region which overlaps with the CO 4σ and 5σ states at the low-energy side below 525 eV, although the qualitative conclusions through spectral finger-printing remain valid at the high-energy side.
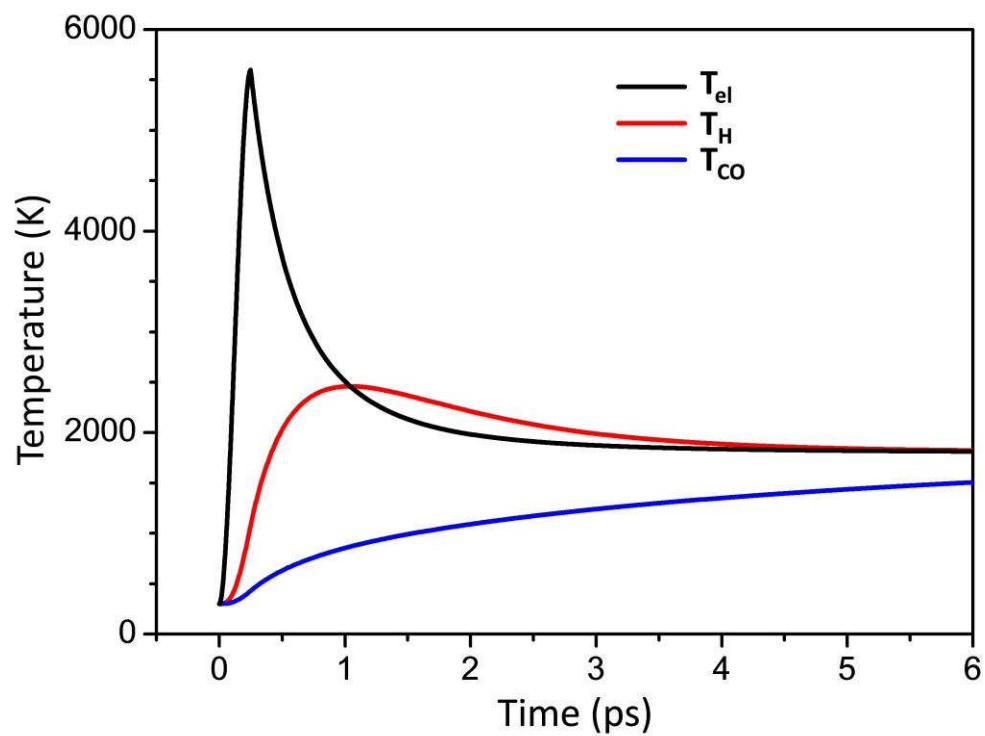
Figure S1. The time evolution of the electronic temperature (T_{el}), H(ads) temperature (T_H), and CO(ads) temperature (T_{CO}) based on the two-temperature model(32) are shown.
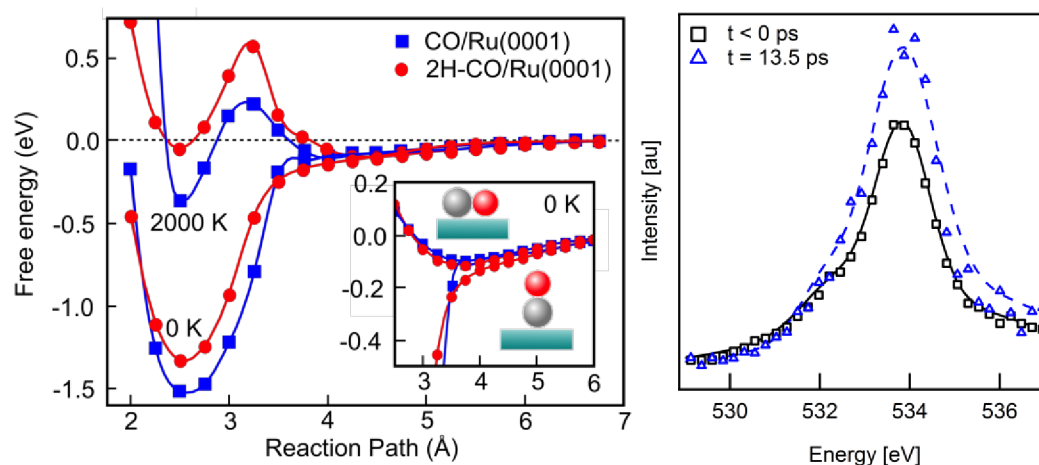
Figure S2. (left) The free-energy diagram for CO on Ru(0001) in the presence and absence of H atoms for 0 and 2000 K. Similar to CO on Ru(0001),(30) the precursor state is present in the free-energy diagram. **(right)** O K-edge XAS at negative delay for the unpumped system and at 13.5 ps after laser excitation showing the increase in intensity of the $2\pi^*$ peak. The increase in intensity is observed at t > 6 ps and remains present at t = 66 ps, the longest timescale measured. The precursor state is the result of a shallow potential well due to an entropic barrier for the CO molecules to adsorb on the surface.(33) The distance-dependent change in entropy of CO gives rise to the barrier between the precursor and chemisorbed states. At distances close to the surface (< 4 Å), CO has a preferential orientation with the C atom pointed down towards the surface and the O atom towards vacuum, while the horizontal orientation, with the C and O equidistant from the surface, is highly repulsive. At far distances (> 4 Å), the energetics of these two orientations converge so that there is no orientation dependence, allowing the CO more degrees of freedom and an increase in entropy.
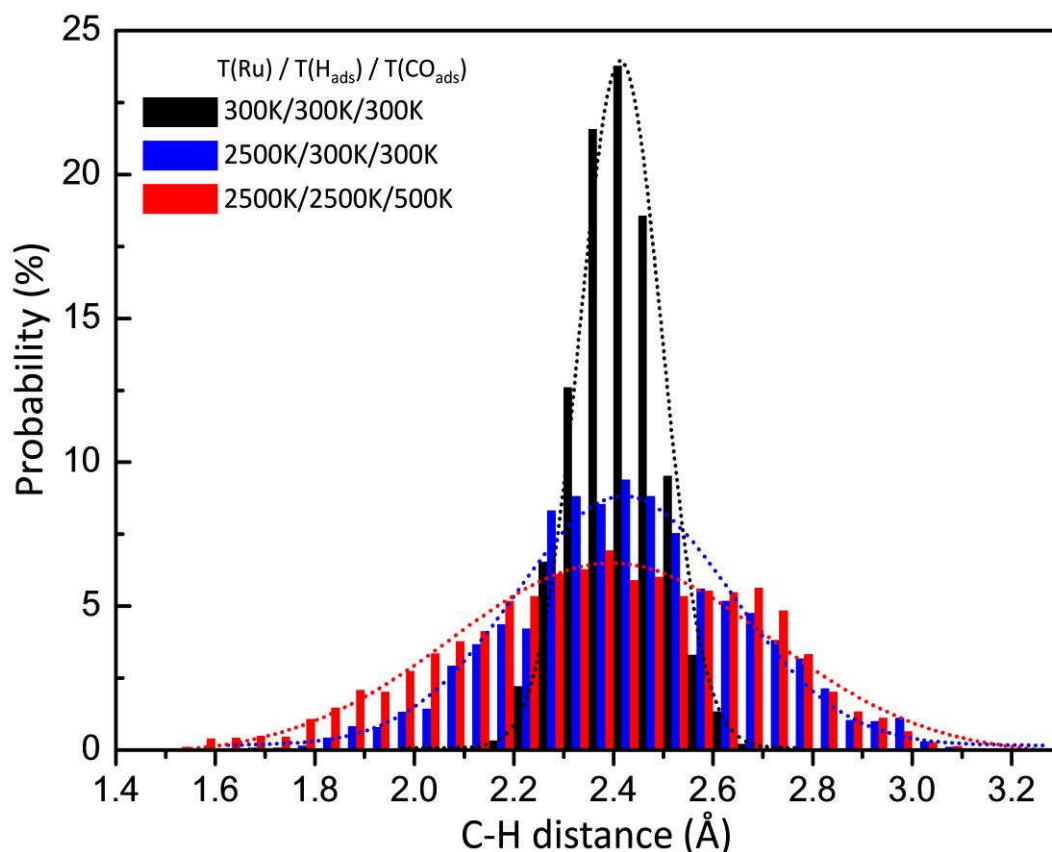
Figure S3. The probability distributions of the shortest C-H distances for CO + H on Ru(0001) during 2.0 ps of molecular dynamics simulations. Three sets of initial temperature (Kelvin) $(T(Ru)/T(H_{ads})/T(CO_{ads}))$, i.e. 300/300/300, 2500/300/300, and 2500/2500/500, were used to simulate the thermal state of the system at different times according to the two-temperature model. The binning of the C-H distances for the statistics is set as 0.05 Å and each red column shares the same values of C-H distance with the blue and black columns on its left side. Under high temperature of H(ads) and CO(ads), there is an increase in the C-H bond length distribution ranging from 1.6 Å to 1.8 Å compared to the low temperature scenario. These distances correspond to populating the pre-transition state (pre-TS) along the reaction coordinate.
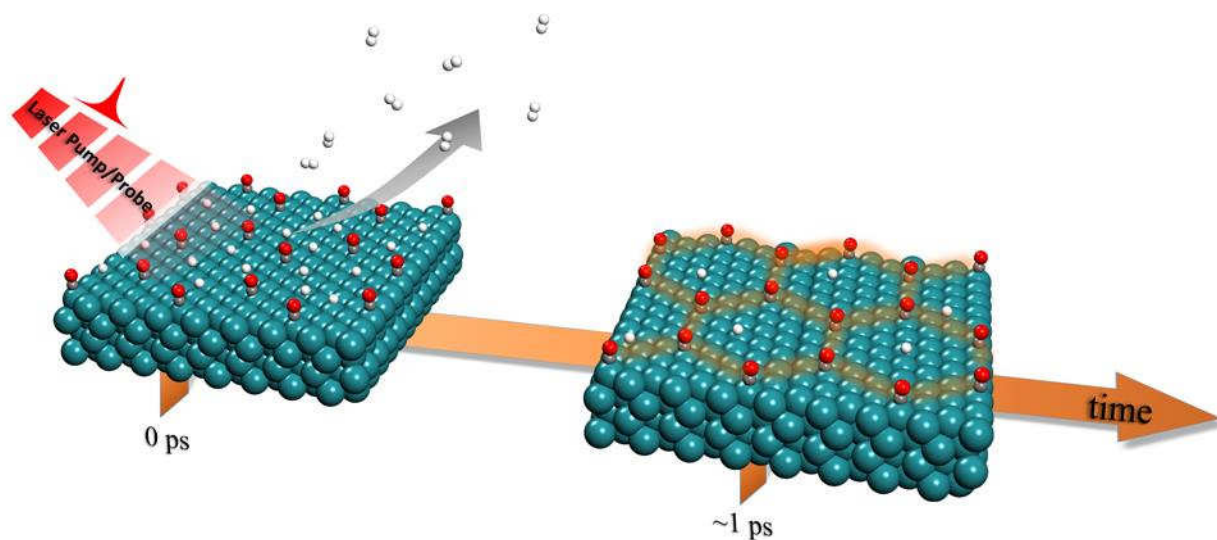
Figure S4. Schematic representation of results of molecular dynamics simulation indicating how the H atoms on the surface get caged by CO molecules after H_2 desorption is initiated. Within the first ps, the coverage of atomic H decreases rapidly as H_2 forms and desorbs. The depletion of atomic hydrogen results in an increased mobility of CO. Due to the mass difference, the hydrogen translational motion is fast compared to the translational motion of CO. Compared to the hydrogen motion CO seems immobile except for the excited rotational motion, in which the tilting geometry of CO increases the probability of interaction with hydrogen leading to the development of the H-CO spectroscopic signal. The potential barrier formed between CO molecules constrains the mean free diffusion length of H atoms and thus increases the probability of interaction between H and CO. On a longer timescale, the increased mobility of CO allows for a fraction of CO entering into the precursor state.
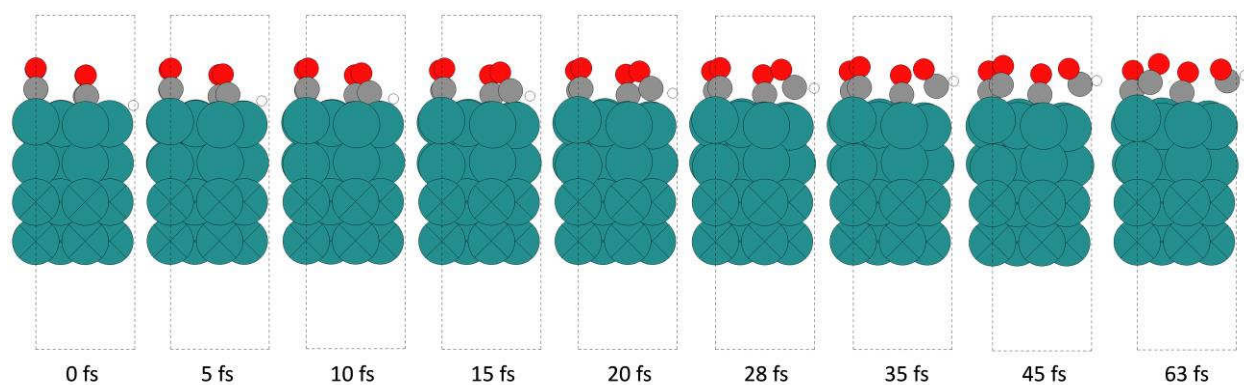
Figure S5. The simulated CHO(ads) formation trajectory using Ab Initio molecular dynamics (AIMD) simulations carried out in the NVT ensemble using Langevin dynamics as implemented in the Atomic Simulation Environment (ASE).
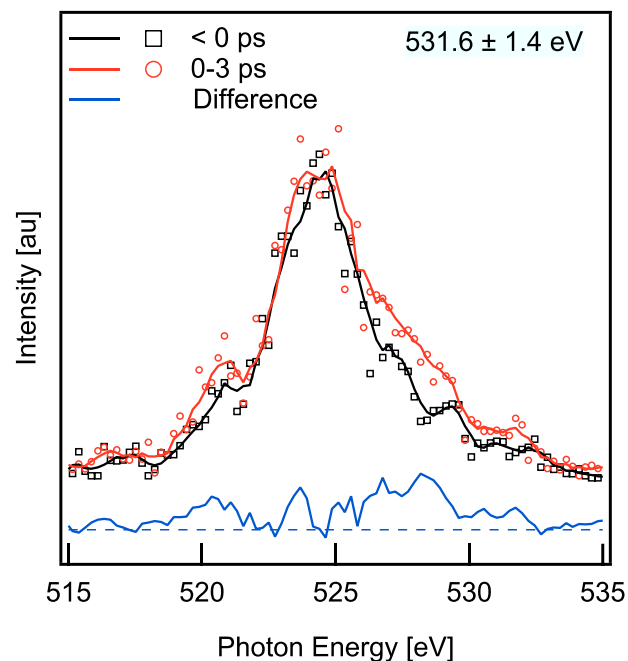
Figure S6. O K-edge XES at negative delay for the unpumped system and at 0.0-3.0 ps after laser excitation, which use the same data set as that used in Figure 1(c). The spectra were normalized to the incoming x-ray photon flux. Solid curves show spectra smoothed with a Gaussian function of 1 eV full width at half maximum to match the instrumental energy resolution. The spectral difference between the two spectra is present also after smoothing the spectra.
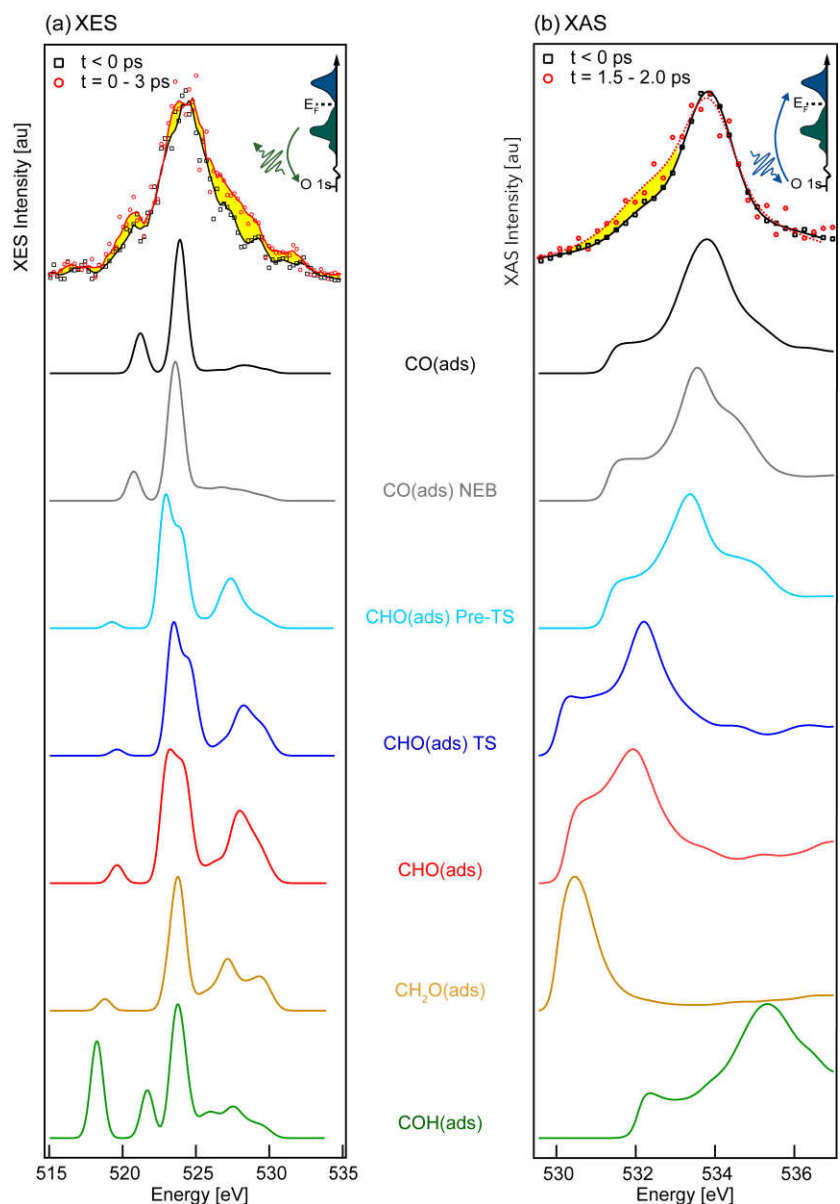
Figure S7. Comparison of experimental O K-edge XES (left) and XAS (right) with computed spectra for CO and different potential intermediates and products. From top to bottom: experimental spectra from Figure 1 of the main text, CO(ads), CO(ads) near the equilibrium state (NEB, H-C distance 2.01 Å), CHO(ads) approaching the transition state (Pre-TS; H-C distance 1.26 Å), CHO(ads) at the transition state (TS; H-C distance 1.15 Å), CHO(ads) (H-C distance 1.11 Å), CH_2O(ads) and COH(ads). It is clear that COH both in XES and XAS would contribute

to a spectral region where no significant changes are observed and that $CH_2O(ads)$ can only make minor contributions.

$H_{ads} + H_{ads} \rightarrow H_{2\,ads}$	
IS	Ru-H: 777.0, 796.4, 840.0, 875.6, 1102.3, 1126.9
TS	Ru-H: 191.1, 290.1, 301.0, 1877.0, 1965.3
FS	Ru-H: 135.0, 315.9, 353.6, 853.8, 1639.3 H-H: 2706.6
$CO(ads) + H(ads) \rightarrow CHO(ads)$	
IS	Ru-CO: 84.3, 229.8, 351.7, 404.9, 444.7 Ru-H: 824.2, 898.6, 1131.5 C-O: 1988.5
TS	Ru-CHO: 146.4, 225.9, 335.1, 399.6, 505.3 C-H: 1027.2, 2222.9 C-O: 1681.9
FS	Ru-CHO: 62.9, 186.3, 231.2, 299.9, 510.3, 754.3 C-H: 1231.5, 2892.2 C-O: 1418.9
$CHO(ads) + H(ads) \, dsCH_2O(ads)$	
IS	Ru-CHO: 128.4, 216.7, 237.6, 371.6, 525.0, 753.7 Ru-H: 746.5, 904.5, 1114.7 C-H: 1238.0, 2920.3 C-O: 1392.7
TS	Ru- CH_2O: 145.6, 240.1, 321.3, 400.0, 1020.6, 1071.4 Ru-H: 2002.9 C-H: 668.3, 1238.7, 3022.1 C-O: 1449.7
FS	Ru- CH_2O: 131.3, 193.9, 250.0, 388.7, 461.6, 623.4 C-O: 886.4, 1101.8, 1155.8 C-H: 1444.1, 2973.9, 3043.6

Table S1. The non-imaginary vibrational frequencies (in cm^{-1}) of the chemical bonds in the initial state (IS), transition state (TS), and final state (FS) of the three competing surface reactions, i.e. H(ads) + H(ads) $\rightarrow$ H$_2$(ads), CO(ads) +H(ads) $\rightarrow$ CHO(ads), and CHO(ads) + H(ads) $\rightarrow$ CH$_2$O(ads).

References to Supporting Information

(1)   Sun, Y. K. and Weinberg, W. H. Determination of the Absolute Saturation Coverage of Hydrogen on Ru(001), *Surf. Sci.* **1989**, *214*, L246-L252, DOI:10.1016/0039-6028(89)90403-2.

(2)   Riedmuller, B., Ciobica, I. M., Papageorgopoulos, D. C., Berenbak, B., van Santen, R. A. and Kleyn, A. W. The Dynamic Interaction of CO with Ru(0001) in the Presence of Adsorbed CO and Hydrogen, *Surf. Sci.* **2000**, *465*, 347-360, DOI:10.1016/S0039-6028(00)00767-6.

(3)   Riedmuller, B., Ciobica, I. M., Papageorgopoulos, D. C., Frechard, F., Berenbak, B., Kleyn, A. W. and van Santen, R. A. CO adsorption on hydrogen saturated Ru(0001), *J. Chem. Phys.* **2001**, *115*, 5244-5251, DOI:10.1063/1.1395625.

(4)   Riedmuller, B., Papageorgopoulos, D. C., Berenbak, B., van Santen, R. A. and Kleyn, A. W. `Magic' Island Formation of CO Coadsorbed with H on Ru(0001), *Surf. Sci.* **2002**, *515*, 323-336, DOI:10.1016/S0039-6028(02)01912-X.

(5)   Katayama, T., T. Anniyev, T., Beye, M., Coffee, R., Dell'Angela, M., Föhlisch, A., Gladh, J., Kaya, S., Krupin, O., Nilsson, A. *et al.* , Nordlund, D., Schlotter, W. F., Sellberg, J. A., Sorgenfrei, F., Turner, J. J., Wurth, W., Öström, H. and Ogasawara, H. Ultrafast Soft X-ray Emission Spectroscopy of Surface Adsorbates Using an X-ray Free Electron Laser, *J. Electron Spectrosc. Relat. Phenom.* **2013**, *187*, 9-14, DOI: 10.1016/j.elspec.2013.03.006.

(6)   Schlotter, W. F., Turner, J. J., Rowen, M., Heimann, P., Holmes, M., Krupin, O., Messerschmidt, M., Moeller, S., Krzywinski, J., Soufli, R. *et al.* The Soft X-ray Instrument for Materials Studies at the Linac Coherent Light Source X-ray Free-Electron Laser, *Rev. Sci. Instrum.* **2012**, *83*, 043107, DOI: 10.1063/1.3698294.

(7)   Dakovski, G. L., Heimann, P., Holmes, M., Krupin, O., Minitti, M. P., Mitra, A., Moeller,
       S., Rowen, M., Schlotter, W. F. *et al.* The Soft X-ray Research instrument at the Linac
       Coherent Light Source, *J. Synchrotron Radiat.* **2015**, *22*, 498-502, DOI:
       10.1107/S160057751500301X.

(8)   Bostedt, C., Boutet., S., Fritz, D., Huang, Z., Lee, H., Lemke, H., Robert, A., Schlotter, W.
       F., Turner, J. J., Williams, G. Linac Coherent Light Source: The First Five Years, *Rev. Mod.
       Phys.* **2016**, *88*, 015007, DOI: 10.1103/RevModPhys.88.015007.

(9)   Tiedtke, K., Sorokin, A. A., Jastrow, U., Juranic, P., Kreis, S., Gerken, N., Richter, M., Arp
       U., Feng, Y., Nordlund, D. *et al.* Absolute Pulse Energy Measurements of Soft X-rays at
       the Linac Coherent Light Source, *Opt. Express* **2014**, *22*, 21214-21226, DOI:
       10.1364/OE.22.021214.

(10)   Heimann, P., Krupin, O., Schlotter, W. F., Turner, J., Krzywinski, J., Sorgenfrei, F.,
       Messerschmidt, M., Bernstein, D., Chalupsky, J., Hajkova, V. *et al.* Linac Coherent Light
       Source Soft X-ray Materials Science Instrument Optical Design and Monochromator
       Commissioning, *Rev. Sci. Instrum.* **2011**, *82*, 093104, DOI:10.1063/1.3633947..

(11)   Gahl, C., Azima, A., Beye, M., Deppe, M., Doebrich, K., Hasslinger, U., Hennies, F.,
       Melnikov, A., Nagasono, M., Pietzsch, A. *et al.* A femtosecond X-ray/optical Cross-
       correlator, *Nat. Photonics* **2008**, *2*, 165-169, DOI: 10.1038/nphoton.2007.298.

(12)   Beye, M., Krupin, O., Hays, G., Reid, A. H., Rupp, D., de Jong, S., Lee, S., Lee, W. S.,
       Chuang, Y. D., Coffee, R. *et al.* X-ray Pulse Preserving Single-shot Optical Cross-
       correlation Method for Improved Experimental Temporal Resolution, *Appl. Phys. Lett.*
       2012, *100*, 121108, DOI:10.1063/1.3695164.

(13) Gladh, J., Hansson, T. and Öström, H. Electron- and Phonon-coupling in Femtosecond
      Laser-induced Desorption of CO from Ru(0001), *Surf. Sci.* **2013**, *615*, 65-71, DOI:
      10.1016/j.susc.2013.05.002.

(14) Denzler, D. N., Frischkorn, C., Wolf, M. and Ertl, G. Surface Femtochemistry: Associative
      Desorption of Hydrogen from Ru(001) Induced by Electronic Excitations, *J. Phys. Chem. B*
      2004, 108, 14503-14510, DOI:10.1021/jp049199i.

(15) Mortensen, J. J., Hansen L. B. and Jacobsen K. W. Real-space Grid Implementation of the
      Projector Augmented Wave Method, *Phys. Rev. B* **2005**, *71*, 035109, DOI:
      10.1103/PhysRevB.71.035109.

(16) Enkovaara, J., Rostgaard, C., Mortensen, J. J., Chen, J., Dułak, M., Ferrighi, L., Gavnholt,
      J. , Glinsvad, C., Haikola, V., Hansen, H. A. *et al.* Electronic Structure Calculations with
      GPAW: a Real-space Implementation of the Projector Augmented-wave Method, *J. Phys.:*
      Condens. Matter **2010**, *22*, 253202, DOI:10.1088/0953-8984/22/25/253202.

(17) Blöchl, P. E. Projector Augmented-wave Method, *Phys. Rev. B* **1994**, *50*, 17953-17979,
      DOI:10.1103/PhysRevB.50.17953.

(18) Hammer, B., Hansen, L. B. and Nørskov, J. K. Improved Adsorption Energetics within
      Density-functional Theory Using Revised Perdew-Burke-Ernzerhof Functionals, *Physl Rev.*
      B **1999**, *59*, 7413-7421, DOI: 10.1103/PhysRevB.59.7413.

(19) Haydock, R., Heine, V. and Kelly, M. J, Electronic Structure Based on the Local Atomic
      Environment for Tight-binding Bands, *J. Phys. C* **1972**, *5*, 2845-2858, DOI: 10.1088/0022-
      3719/5/20/004.

(20) Triguero, L., Pettersson, L. G. M. and Ågren, H. Calculations of Near-edge X-ray-
      Absorption Spectra of Gas-phase and Chemisorbed Molecules by Means of Density-

Functional and Transition-potential Theory, *Phys. Rev B* **1998**, *58*, 8097-8110, DOI: 10.1103/PhysRevB.58.8097.

(21) Ljungberg, M. P., Mortensen J. J. and Pettersson, L. G. M. An Implementation of Core Level Spectroscopies in a Real Space Projector Augmented Wave Density Functional Theory Code, *J. Electron Spectrosc. Relat. Phenom.* **2011**, *184*, 427-439, DOI:10.1016/j.elspec.2011.05.004.

(22) Föhlisch, A., Hasselström, J., Bennich, P., Wassdahl, N., Karis, O., Nilsson, A., Triguero, L., Nyberg, M. and Pettersson, L. G. M. Ground-state Interpretation of X-ray Emission Spectroscopy on Adsorbates: CO Adsorbed on Cu(100), *Phys. Rev. B* **2000**, *61*, 16229-16240, DOI:10.1103/PhysRevB.61.16229.

(23) Monkhorst, H. J. and Pack, J. D. Special Points for Brillouin-zone Integrations, *Phys. Rev. B* **1976**, *13*, 5188-5192, DOI:10.1103/PhysRevB.13.5188.

(24) Berne, B. J., Ciccotti, G. and Coker, D. F., *Classical and Quantum Dynamics in Condensed Phase Simulations;* World Scientific Publishing: Singapore, Singapore; 1998.

(25) Sheppard, D., R. Terrell, R. and Henkelman, G. Optimization Methods for Finding Minimum Energy Paths, *J. Chem. Phys.* **2008**, *128*, 134106, DOI:10.1063/1.2841941.

(26) Giannozzi, P., Baroni, S., Bonini, N., Calandra, M., Car, R., Cavazzoni, C., Ceresoli D., Chiarotti, G. L., Cococcioni, M., Dabo, I. et al. QUANTUM ESPRESSO: a Modular and Open-source Software Project for Quantum Simulations of Materials, *J. Phys.: Condens. Matter* **2009**, 21, 395502.

(27) Wellendorff, J., Lundgaard, K. T., Møgelhøj, A., Petzold, V., Landis, D. D., Nørskov, J. K., Bligaard T. and Jacobsen, K. W. Density Functionals for Surface Science: Exchange-

correlation Model Development with Bayesian Error Estimation, *Phys. Rev. B* **2012**, *85*, 235149, DOI:10.1103/PhysRevB.85.235149.

(28) Doren, D. J. and Tully, J. C. Precursor-Mediated Adsorption and Desorption: a Theoretical Analysis, *Langmuir* **1988**, *4*, 256-268, DOI:10.1021/la00080a004.

(29) Doren, D. J. and Tully, J. C., Dynamics of precursor-mediated chemisorption, *J. Chem. Phys.* **1991**, *94*, 8428-8440, DOI:10.1063/1.460076.

(30) Dell'Angela, M., Anniyev, T., Beye, M., Coffee, R., Föhlisch, A., Gladh, J., Katayama, T., Kaya, S., Krupin, O., LaRue, J. *et al.* Real-Time Observation of Surface Bond Breaking with an X-ray Laser, *Science* **2013**, *339*, 1302-1305, DOI:10.1126/science.1231711.

(31) Öberg, H., Gladh, J., Dell'Angela, M., Anniyev, T., Beye, M., Coffee, R., Föhlisch, A., Katayama, T., Kaya, S., Larue, J. *et al.* Optical Laser-induced CO Desorption from Ru(0001) Monitored with a Free-electron X-ray Laser: DFT Prediction and X-ray Confirmation of a Precursor State, *Surf. Sci.***2015**, *640*, 80-88, DOI:10.1016/j.susc.2015.03.011.

(32) Anisimov, S. I., Kapeliov, B. L. and Perel'man, T. L. Electron Emission from Metal Surfaces Exposed to Ultrashort Laser Pulses, J. Exp. Theor. Phys.. **1974**, *39*, 375-377.

(33) Xin, H., LaRue, J., Öberg, H., Beye, M., Dell'Angela, M., Turner, J. J., Gladh, J., Ng, M. L., Sellberg, J. A., Kaya, S. *et al*. Strong Influence of Coadsorbate Interaction on CO Desorption Dynamics on Ru(0001) Probed by Ultrafast X-Ray Spectroscopy and Ab Initio Simulations, *Phys. Rev. Lett.* **2015**, *114*, 156101, DOI:10.1103/PhysRevLett.114.156101.